16th World Conference on Earthquake, 16WCEE 2017

Santiago Chile, January 9th to 13th 2017

Paper N° 1943

Registration Code: S-B1463055888

Fundamental Study Using New Test Loading Scheme for Steel Frame Subassembly with Damper Connection Details

Y. Matsuda(1), K. Kasai(2), S. Motoyui(3), S. Kishiki(4)

(1) *Assistant Professor, Tokyo University of Science, matsuda_y@rs.tus.ac.jp*
(2) *Professor, Tokyo Institute of Technology, kasai.k.ac@m.titech.ac.jp*
(3) *Professor, Tokyo Institute of Technology, motoyui.s.aa@m.titech.ac.jp*
(4) *Associate Professor, Tokyo Institute of Technology, kishiki.s.aa@m.titech.ac.jp*

Abstract

The performance of passively controlled buildings depends not only on dampers but also on frame members and connections. The frame members are subjected to bending moments and shear forces caused by the story drift and relatively large axial forces caused by the damper force. The damper force and damper deformation have shifted phases, and the former is in phase with the frame story drift, which produces a phase difference between the moment and the axial force. In addition, the axial force can cause earlier yielding and possibly local buckling in the elements, but very few studies have investigated this problem. Because a detailed method of analyzing the connection elements, such as gusset plates and stiffeners, has not yet been established, buildings are constructed using a variety of designs, including many that are irrational and inadequate. Furthermore, stress concentrations at the gusset plate connecting the damper complicate the beam behavior. In this study, this was considered by analyzing data from beam–column–gusset plate subassembly tests.

The subassembly test performed in this study employed a newly developed loading method alternating displacement control for story drift and force control for the damper force, the target value of which is calculated over a number of steps based on a hybrid scheme using a numerical model of the damper. Tests were conducted on 10 subassemblies consisting of a beam, a column, and a gusset plate, and the results were analyzed and discussed. When analyzing the data, two contributions containing the phases of the story drift and damper force were extracted from each of the forces shared by the steel beam and gusset plate and their corresponding strains. This paper discusses the results and their implication to the analysis and design of the members and connections in the damper.

Some of the results are given below.

- The proposed test method for the subassembly with simulated frame and damper actions performed well, producing realistic overall hysteresis and local behavior. Simultaneous displacement and force control, connected by the numerical simulation of the damper action, was performed.
- The gusset plate designed to satisfy the requirements of a conventional brace frame failed prematurely, demonstrating the inadequacy of the conventional method. The stiffeners around the connection greatly influence the stress transfer in the gusset plate. Many specimens exhibited local buckling at the bottom flange on the outside edge of the gusset plate.
- Two-dimensional strains at the gusset plate of the subassembly were decomposed from the recorded strains into the frame and damper action components based on the phase difference between the two actions, and highly non-uniform strains were clarified by a combination of the two scaled actions. It was demonstrated that the contribution of each action could be obtained without conducting a separate test, and the combined effects can be easily evaluated for design.

Keywords: Passive control, Steel building, Gusset plate

1. Introduction

Passively-controlled building is suitable for a steel frame because of ease for connecting dampers and relatively low frame stiffness requiring drift control. The typical form includes a damper in the gusset plate, which is installed on the diagonal of the frame [1-4]. The connection form is similar to that in a conventional building. The design concept of passively controlled buildings differs from that of conventional buildings. During a major earthquake, the former is designed to remain almost elastic, and the latter is permitted to undergo significant inelastic deformations as long as it does not collapse. One conventional building type includes concentric braces, and the brace connection details are often utilized in passively controlled buildings with brace-type dampers. Obviously, this is inappropriate because such a design permits the yielding of the components and does not limit deformation.

The purpose of this paper is to examine the effects of the parameters of connection details as well as the types and sizes of dampers that can generate stresses with different phases and magnitudes in the connections. To serve this purpose, a new experimental method was developed as an efficient tool for conducting tests with the variation of the many parameters indicated above. The experimental method was conducted using a compact system with simultaneous displacement and load control, which reproduce the story drift and damper force, respectively, of the full-scale subassembly.

2. FULL-SCALE SUBASSEMBLY TESTS

2.1 Outline of Hybrid Test Combining Frame and Damper Actions

Figure 1 shows the concept of a simplified hybrid test method combining frame and damper actions. The subassembly has an L-shaped configuration, representing a quarter of the frame. Figure 2 shows the three types of dampers considered in this study (steel, viscoelastic, and friction dampers) and their deformations u_d. The frame members were subjected to bending moments and shear forces caused by story drift and relatively large axial forces caused by the damper force. Therefore, the beam axial force and moment have different phases and time lags. The proposed test method can simulate these effects.

Figure 3 shows the loading method, which is as follows. First, the story drift is applied to the specimen by the displacement control unit while maintaining a constant damper force (Figure 3a). Second, the target damper force is calculated according to the change in the diagonal distance and is used as the input of the force control unit, which ultimately produces the specified damper force (Figure 3b). The target story drift u reflects the frame action, and the target damper force F_d reflects the damper action. The target F_d depends on the change Δu_a in the diagonal distance due to local deformations, such as gusset plate yielding and the axial contraction of the

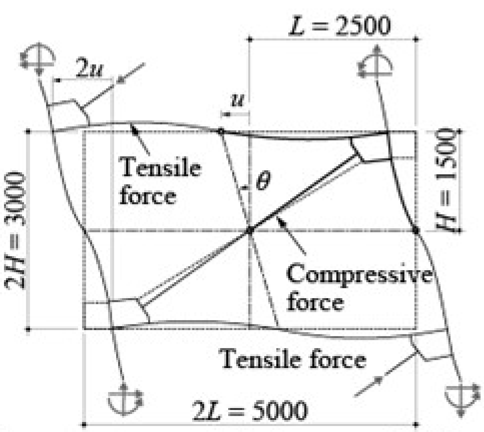

Figure 1 Assumed displacement field for simplified hybrid test method (unit:mm)

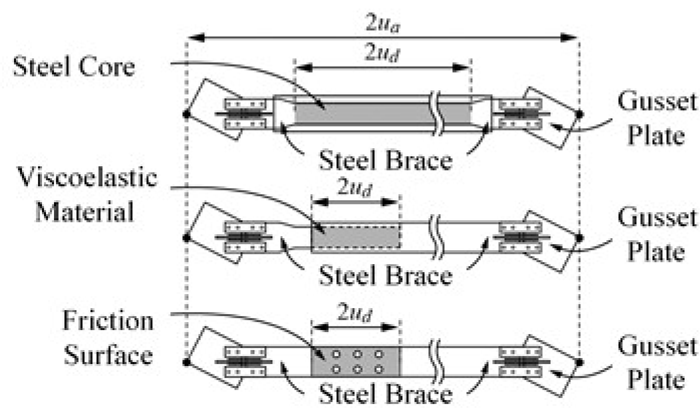

Figure 2 Three types of dampers (steel, viscoelastic, and friction damper) and those deformations.

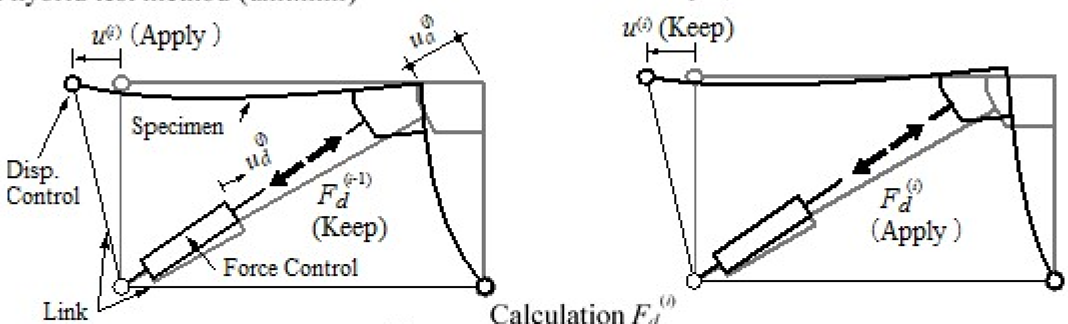

(a) Apply $u^{(i)}$, keep $F_d^{(i-1)}$ (b) Keep $u^{(i)}$, apply $F_d^{(i)}$

Figure 3 Loading method in i-th step

beam as a result of local buckling. The target F_d is calculated by substituting the measured Δu_a into the mathematical model of the damper (virtual damper) at every step of the test. Figure 4 shows the test setup, in which the laterally supported L-shaped specimen is connected to two links that maintain constant distances between the midpoint of the brace and the inflection points in the beam and column. Two parallel actuators (total capacity of 3,000 kN) were used to control the displacement and satisfy the target story drift u or story drift angle $\theta = u/H$, and one oil jack (capacity of 1,000 kN) was diagonally placed to control the force and simulate the damper force F_d.

Figure 5 shows the loading protocol. The magnitude of the story drift angle θ was cyclically increased in both the positive and negative directions. In addition, because significant damage was expected in Specimen 4, it is mentioned in Node 2.2, and thus $\theta = \pm 1/40$ rad was added to the story drift angle of Specimen 4. Specimens 1, 9, and 10 were loaded with multiple cycles of $\theta = \pm 1/50$ rad until failure. Specimens 2 to 8 were loaded with multiple cycles of $\theta = \pm 1/33$ rad until failure.

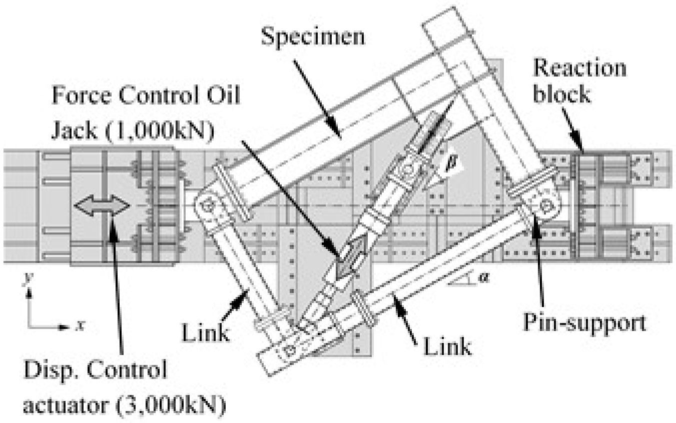

Figure 4 Test set-up

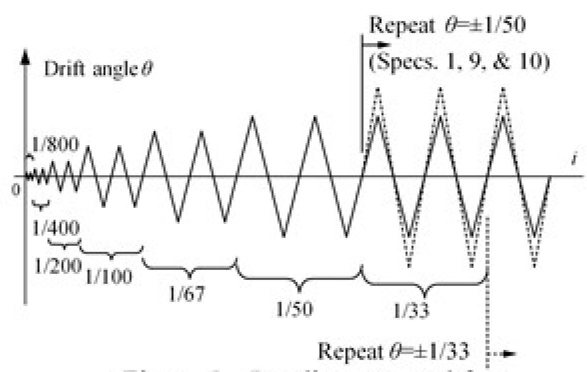

Figure 5 Loading protocol for frame action protocol

2.2 Specimen Scheme

Figure 6a shows a standard specimen. Each specimen consists of a steel beam (BH-500×250×12×22), a column (□-400×400×19), a gusset plate (PL-19 mm), and four types of stiffeners (PL-16 mm). The beam, vertical and horizontal side, and column stiffeners were welded to the beam, gusset plate, and column, respectively, as shown in Figure 6b.

Table 1 lists the specimen types and their characteristics. Specimens 1 to 3, which are all standard specimens as defined by Japanese criteria [9], were subjected to a steel damper force after the Menegotto–Pinto model [5, 6], a viscoelastic damper forces [7], and a friction damper force, respectively. A steel damper force

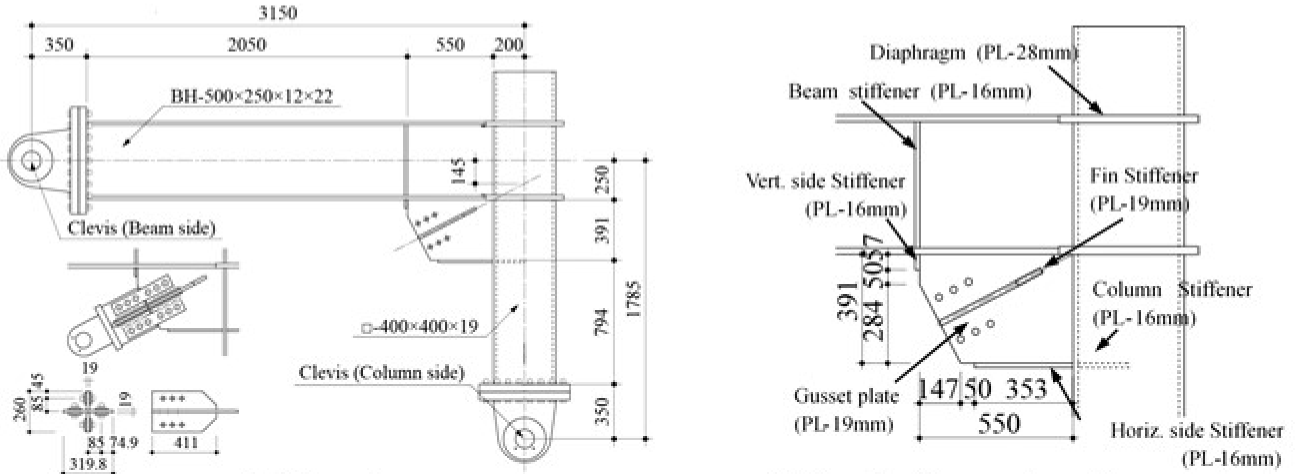

(a) Overall (b) Details of connection with gusset plate

Figure 6 Standard type full-scale subassembly specimen (unit:mm)

8	No column, beam or horiz. and vert. stiffeners.
9	No danper force.
10	No gusset plate, stiffeners, or damper force.

* Steel damper for fatigue test

	3	280.3	66600	3330	12330	1515	1801

was applied to Specimen 2 at $\theta = \pm 1/33$ rad. Table 2 gives the properties of the member cross sections of the specimens. The web (9 mm) of Specimen 4 is thinner than that of the standard specimen. This specimen does not meet the Japanese code requirements for a beam–column compact section [8] and barely satisfies the requirements for a beam. The web (9 mm) and flange (16 mm) of Specimen 5 are both thinner than those of the standard specimen, and the flange slightly violates the compact section requirement for a beam. The thickness of the gusset plate of Specimen 6 is 9 mm, which is less than half that of the standard specimen and based on Japanese criteria [9]. Specimen 7 does not contain horizontal or column stiffeners (Figure 6b), and Specimen 8 has no stiffeners at all. Specimen 9 was not subjected to a damper force. Specimen 10 does not contain a gusset plate or stiffeners and was not subjected to a damper force.

2.3 Measurement scheme

Figure 7 shows the definition of the deformation and stress in the positive and negative loading cases. The positive (negative) loading case is defined as causing a positive (negative) moment and axial tension (compression) in the beam. The section forces were calculated under equilibrium conditions in Figure 7a from the angles of inclination α (= 29.54°) and β (= 27.50°) (Figure 4), the actuator force F, and the oil jack force F_d. The section forces are expressed as

$$Q_b = F \cdot \sin\alpha - F_d \cdot \sin\beta \quad , \quad N_b = F \cdot \cos\alpha \quad , \quad Q_s = N_b$$
$$Q_c = F \cdot \cos\alpha - F_d \cdot \cos\beta \quad , \quad N_c = F \cdot \sin\alpha \quad , \quad Q_f = Q_c \qquad \text{(1a-f)}$$

where Q_s is the shear force of the system (with frame and damper combined in parallel) and Q_f is the shear force of the subassembly.

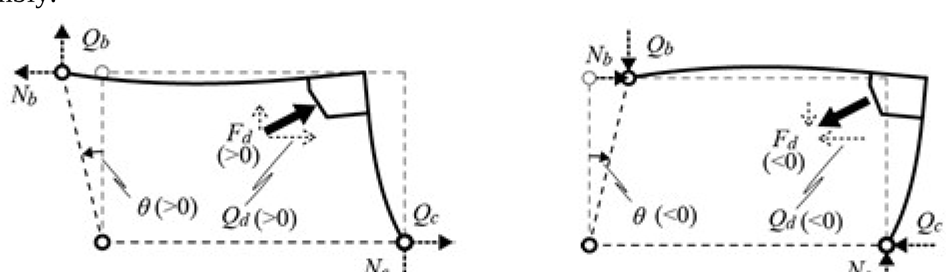

(a) Positive loading case (b) Negative loading case

Figure 7 Definitions of deformation and stress

The story drift u, the story drift angle θ, and the deformation u_a of the added component (combining the damper and gusset plate deformations in series) were calculated from the absolute displacements u_{x1} and u_{x3} (Figure 4), the stroke u_{a1} of the oil jack, and the gusset plate deformation u_{a2} as

$$u = \frac{u_{x3} - u_{x1}}{\cos\alpha} \quad , \quad \theta = \frac{u}{H} \quad , \quad u_a = u_{a1} + u_{a2} \qquad \text{(2a-c)}$$

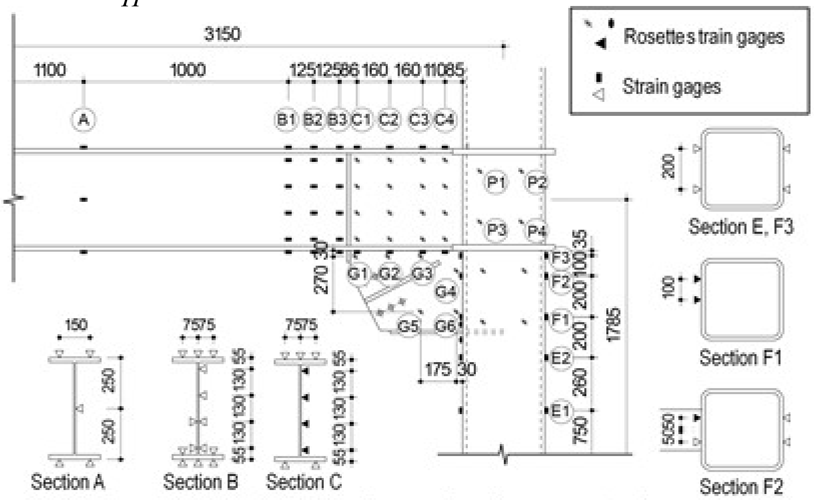

Figure 8 Locations of strain gages (unit:mm)

Figure 8 shows the locations of strain gage. In beam, strain gages were attached to four kind sections. Maintaining elastic until the failure occurs is Section A, section that the large damage will occur is Section B (B1 to B3), section with gusset plate is Section C (C1 to C4). In column, strain gages were attached to two kind sections. Maintaining elastic until the failure occurs is Section E (E1 and E2), section with gusset plate is Section F (F1 to F3). In gusset plate and panel, strain gages are attached to six and four points, respectively, by rosette gage.

3. HYSTERIC BEHAVIOR

3.1 Test Results of Three Kind Damper Force

Figure 9 shows the test results for Specimens 1 to 3. The virtual dampers in these specimens were the steel, viscoelastic, and friction dampers, respectively. The horizontal component Q_d of the damper force, the horizontal force Q_f of the frame, and the horizontal force Q_s of the system are shown. The target Q_d and applied Q_d are shown in the same graph as solid gray and black lines, respectively. As shown in Figures 9a and b, the force control of the virtual steel and viscoelastic dampers was reasonably accurate. Note that for the friction damper, the calculated target force F_d was too sensitive to Δu_a (Figure 3) during unloading because of its large elastic stiffness. Thus, instead of calculating the target F_d, the sign of the slip force F_{dy} was reversed, and the resulting value was used as the target F_d. This resulted in rigid plastic damper performance, causing abrupt changes in strains in the subassembly. Such behavior is considered to demonstrate the extreme and interesting case of the elastoplastic damper and was investigated further.

The frame action can be observed from the Q_f–θ curves in Figure 9. The first yielding occurred at approximately $\theta = \pm 1/200$ rad because of the stress concentration at the bottom flange immediately outside the gusset plate connection. A significant reduction in horizontal stiffness occurred as a result of further beam yielding at $\theta = \pm 1/100$ rad. As will be shown later, the beam fully yielded at $\theta = \pm 1/67$ rad and remained stable at drift angles of up to $\theta = \pm 1/50$ rad and larger except for some specimens. Figure 10 shows that beams of all three systems reach full plasticity at $\theta = \pm 1/67$ rad and $N/N_y \approx 0.25$. Among the three systems, the yielding of the beam was most significant in the system with the friction damper, as suggested by the large beam moment even after unloading shown in Figure 10.

Because the subassembly is L-shaped, the M–N relationship was analogous to the Q_s–θ relationship. The relatively large widths of these loops indicate the extent of the phase difference between the force and deformation and the corresponding equivalent damping of the system. The system using the friction damper with an idealized rigid unloading stiffness yielded the largest energy dissipation and damping. Figure 10 shows that beams of all three systems reach full plasticity at $\theta = \pm 1/67$ rad and $N/N_y \approx 0.25$. Among the three systems, the yielding of the beam was most significant in the system with the friction damper, as suggested by the large beam moment even after unloading shown in Figure 10.

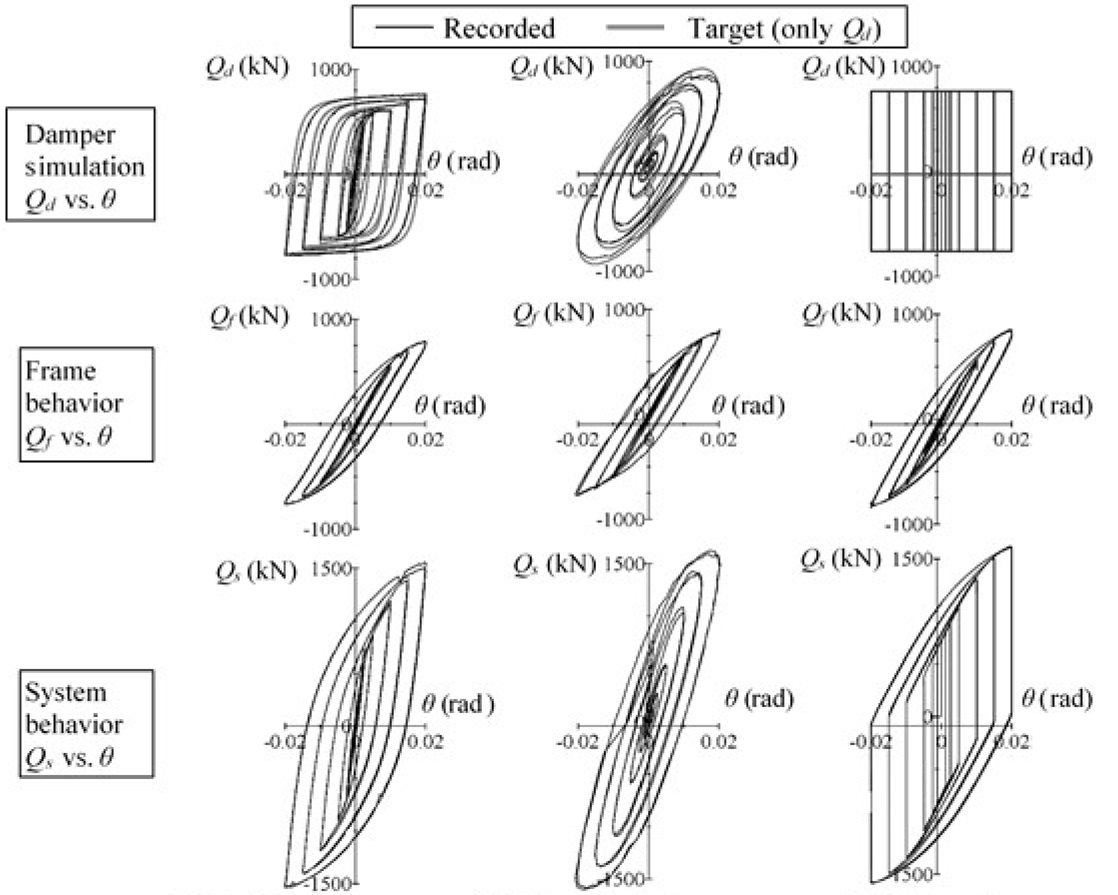

(a) Steel damper (b) Viscoelastic damper (c) Friction damper

Figure 9 Test results for damper, frame, and system action (three types of dampers)

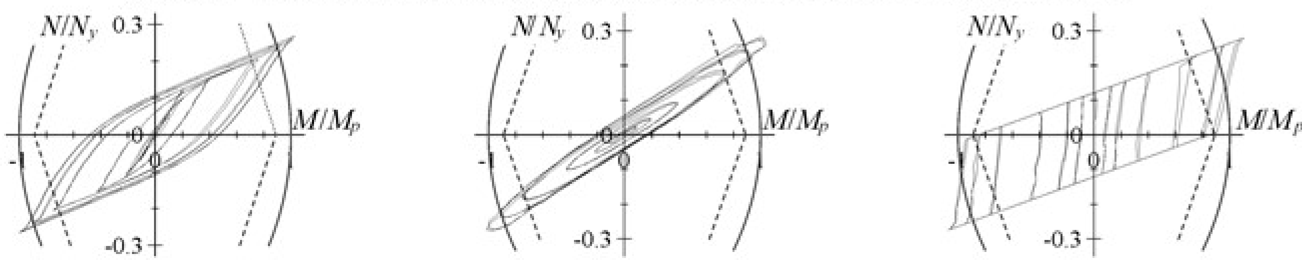

(a) Steel damper (b) Viscoelastic damper (c) Friction damper

Figure 10 Interaction between normalized beam moment M/M_p and normalized axial force N/N_y

3.2 Test Results of All Specimens

Figure 11 shows the Q_f–θ relationship until the maximum drift angle θ was reached; that is, the results of Specimen 9 are shown until θ = 1/50 rad, and those of all other specimens are shown until θ = 1/33 rad. The broken line in each graph shows the calculated value of the yield strength defined as the strength at which the beam reaches the full plastic bending moment assuming F_d = 0, and N_b = 0. Table 3 gives the initial stiffness obtained from the skeleton curve shown in Figure 12, which is discussed later in this section, and the ultimate strength.

Until θ = ±1/50 rad, Specimen 2, which was subjected to viscoelastic damping, experienced approximately the same damage as Specimen 1, which was subjected to steel damping (discussed later). Hence, it was subjected to a steel damper force at θ = ±1/33 rad. In Specimen 2, local buckling occurred from the first cycle of θ = ±1/33 rad, and thus its ultimate strength in the negative loading case was 0.92 times that in the positive loading case (Table 3).

As shown in Figure 11b, Specimen 5, which is the specimen with both a flange and web that are thinner than those of the standard specimen, exhibited the smallest peak story shear due to local buckling. The peak force of this specimen in the negative loading case decreased to 0.52 times the largest peak force during the application of the cyclic deformation with increasing peak drift angle prior to the application of $\theta = -1/33$ rad. In addition, the ultimate strength in the negative loading case was 0.78 times that in the positive loading case (Table 3), and the difference between the two loading cases was the most significant among the specimens.

Specimen 6, which has a thin gusset plate, had a horizontal stiffness similar to that of the standard specimen (Figure 11c). In Specimen 8, which has no stiffeners, the beam deformation decreased as a result of the increased deformation at the column skin plate (Figure 11d).

The beam axial force of Specimen 9, which experienced no damper force, increased in proportion to θ. Therefore, the damage to the beam was small, and because the drift angle of Specimen 9 did not reach $\theta = \pm 1/33$ rad, local buckling did not occur. Hence, the damage to the beam had little influence on the behavior of the frame action, and the ultimate strength of Specimen 9 was larger than that of the standard specimen (Figure 11e).

Figure 12 shows the skeleton curve obtained from the Q_f–θ relationship until the maximum θ. The initial stiffness and ultimate strength of Specimen 3 were larger than those of Specimens 1 and 2 (Table 3). In Specimen 3, the frame shear force Q_f increased because the friction damper force was reversed at unloading. It is considered that the relatively large Q_f of Specimen 3 caused by this friction damper behavior led to a large strain

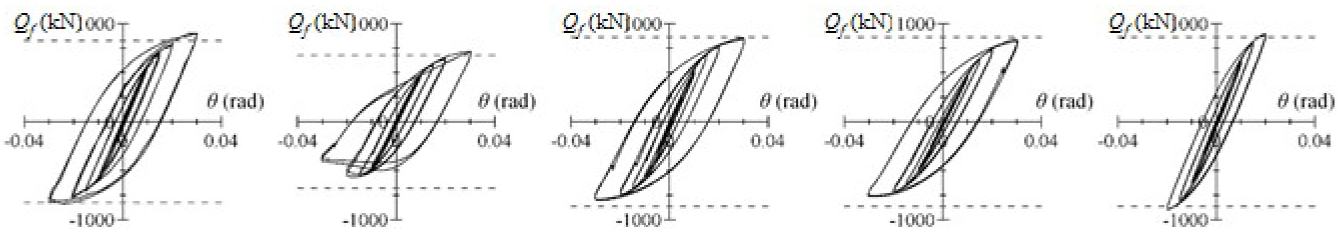

(a) Specimen 2 (Standard specimen) (b) Specimen 5 (Thin web and flange) (c) Specimen 6 (Thin gusset plate) (d) Specimen 8 (No stiffeners) (e) Specimen 9 (No damper)

Figure 11 Skeleton curve obtained by Q_f vs. θ (until θ=1/33, until θ=1/50 only in specimen 9)

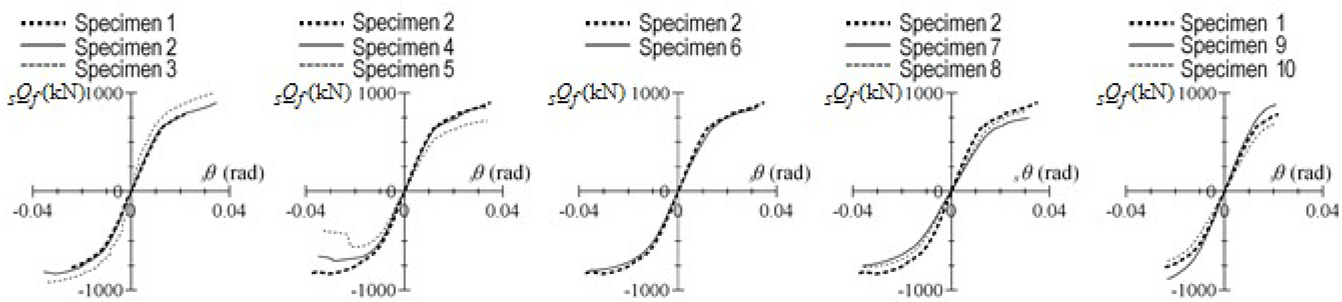

(a) Damper force (b) Width-thickness ratio (c) Gusset plate thickness (d) Presence of stiffeners (e) Application of damper force or presence of gusset plate

Figure 12 Skeleton curve obtained by Q_f vs. θ (until θ=1/33, until θ=1/50 only in specimen 9)

Table 3 Initial stiffness obtained from skeleton curve and ultimate strength

Specimen No.	Initial Stiffness (kN/mm)	Maximum Q_f (kN)	Minimum Q_f (kN)	Specimen No.	Initial Stiffness (kN/mm)	Maximum Q_f (kN)	Minimum Q_f (kN)
1	32.9	802	-767	6	31.3	857	-801
2	35.3	909	-837	7	24.3	784	-757
3	53.8	1009	-921	8	26.8	861	-764
4	31.2	861	-703 ※1	9	36.2	922	-915
5	26.8	719	-562 ※2	10	25.9	705	-709

: Repeated θ=±1/50 until failure ※1 At cycle of θ=±1/40 rad ※2 At cycle of θ=±1/50 rad at the gusset plate and strain hardening, ultimately causing the yield stress of this specimen to be 11% larger than those of the other specimens. Although Specimens 1 and 2 were subjected to different damper forces, their skeleton curves almost coincided until $\theta = \pm 1/50$ rad. In addition, the magnitudes of the strains at the beam and gusset plate were also similar. Therefore, it was assumed that both specimens experienced approximately the same damage until $\theta = \pm 1/50$ rad.

In Specimens 4 and 5, the initial stiffness and ultimate strength were smaller than those of the standard specimens, and these tendencies were consistent with the section properties (Figure 12b and Table 2). As described above, the strength in the negative loading case decreased as the width-to-thickness ratio increased.

In Specimen 6, the initial stiffness and ultimate strength were 0.9 times those of Specimen 2 (Figure 12c); therefore, both specimens showed approximately the same behavior until $\theta = \pm 1/50$ rad. Specimen 9 suffered from early yielding at a cycle of $\theta = 1/200$ rad, whereas the gusset plate of the other specimens yielded at a cycle of $\theta = 1/100$ rad.

In Specimens 7 and 8, the initial stiffness and ultimate strength were smaller than those of Specimen 2 (Figure 12d). Furthermore, because those were smaller than Specimen 5 with both a thinner flange and web (Table 3), the effect of the stiffeners is important.

In Specimen 9, the initial stiffness was similar to those of Specimens 1 and 2 (Figure 12e). However, the ultimate strength was larger than that of Specimen 1 because the damage to the beam was insignificant as a result of the relatively small beam axial force. In addition, the initial stiffness of Specimen 9 was 1.4 times that of Specimen 10, which did not contain the gusset plate or any stiffeners.

4. LOCAL BEHAVIOR OF CONNECTION WITH GUSST PLATE

4.1 Two Separate Tests for Validation of Strain Behavior

To analyze the strain behavior due to the frame and damper actions, a frame action test with $\theta = \pm 1/200$ rad and $F_d = 0$ and a damper action test with $F_d = \pm 700$ kN and $\theta = 0$ were conducted before Specimen 3.

Figure 13 compares the strain distribution of the recorded and theoretical strains in Sections B1, B3, C1, and C4 (Figure 8), where the theoretical value was obtained using beam theory and the test results of N_b and Q_b. In addition, the theoretical value was evaluated including the gusset plate in Sections C1 and C4 and the horizontal side stiffener in Section C4. In Section B1, the distance of which from the face of the vertical stiffener for the gusset plate is 0.6 times the beam depth, the plane section remains approximately plane in the frame and damper actions. Thus, the theoretical strain corresponded to the recorded value in Section B1. However, in Section B3, the distance of which is only 0.1 times the beam depth, the stress at the bottom flange is concentrated and is approximately twice the stress extrapolated from the strains in the upper half of the section in both the positive and negative loading cases. In Sections C1 and C4, the plane sections do not remain approximately plane under frame and damper actions. Thus, the theoretical strain did not correspond to the recorded strain in Sections B3, C1, and C4.

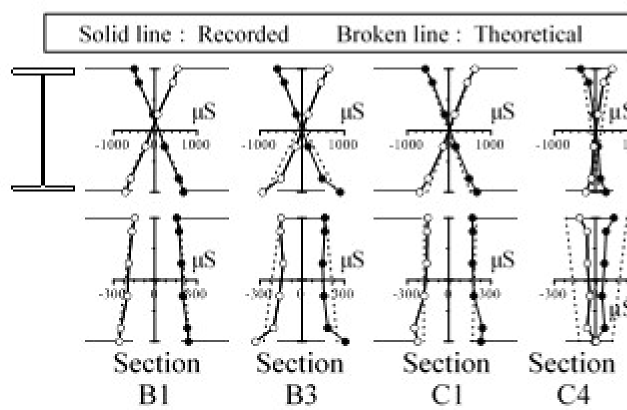

Figure 13 strain distribution of recorded and theoretical value (upper : frame action test, lower : Damper action test)

Figure 14 shows the principle strains obtained in the frame and damper action tests at $\theta = +1/200$ rad and $F_d = -860$ kN, respectively. The direction of the principal strains in the frame action test was approximately the same as that in the damper action test, except in the panel area, where they are opposite. Thus, the strains in the connection increased because of the constructive combination of the two actions, whereas those in the panel decreased. In the gusset plate, the frame action component showed the largest principal strains near the beam flange (960μS) and column face (600μS) at $\theta = +1/200$ rad. In contrast, the damper action component showed only small principal strains. Thus, the gusset plate had a large amount of reserved strength against the damper action. The strain of gusset plate is governed by the frame action and was estimated to yield at $\theta = \pm 1/100$ rad;

however, this could be avoided by simply increasing the plate thickness. The Japanese criteria for the gusset plate consider only the damper force, but it should be modified to consider the frame action discussed here. The strain from the combined frame and damper actions is given by

$$\varepsilon_\alpha = \lambda_\theta \theta + \lambda_F F_d \qquad (3)$$

where ε_α is the strain of arbitrary location and direction due to the sum of the frame and damper actions, λ_θ is the ratio of θ to ε_α and is obtained from the frame action test, and λ_F is the ratio of F_d to ε_α and is obtained from the damper action test. This means that the strain due to the frame and damper actions can be predicted by substituting θ and F_d into Equation 3. Figure 15a compares the recorded strain with the sum of strain from the frame and damper actions. The value of ε_α obtained from Equation 3 was in good agreement with the recorded strain that input the frame and damper actions. Figure 15b shows the recorded and calculated von Mises stresses for $\varepsilon_\alpha = \varepsilon_0$, ε_{45}, ε_{90} at G1 (Figure 11). The recorded and calculated results were in very good agreement. These tests verified that the strain and stress in a frame subjected to story drift and damper forces can be calculated by summing the frame and damper actions.

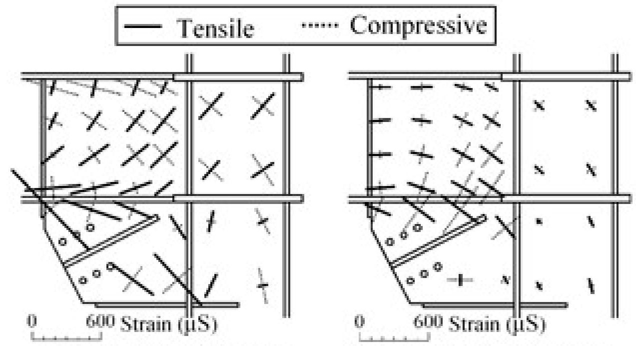

(a) Frame action test at θ=+1/200 rad (b) Damper action test at F_d =-860kN

Figure 14 Separate tests: Recorded principal strains from frame and damper action tests

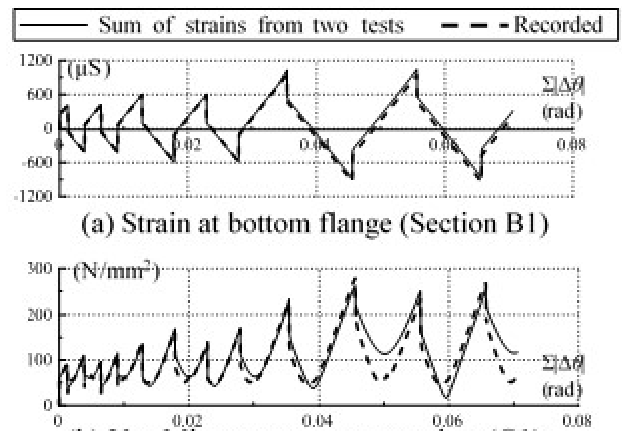

(b) Von Mises stress at gusset plate (G1)

Figure 15 Comparison of sum of strains obtained during frame and damper action tests with recorded strain

4.2 Strain Decomposition

This section proposes a data analysis method to analyze the effect of the frame and damper actions and highly non-uniform strains in the gusset plate connections. Using this method, analysis based on the frame and damper actions is possible without carrying out the two separate tests discussed in Section 4.1. In this method, the frame and damper action components are extracted from the recorded strain ε_i at the *i*-th step. The phases of the frame and damper actions are assumed to be represented by story drift angle θ and the damper force F_d, respectively. The coefficients λ_θ and λ_F that minimize R in the following equation are then obtained:

$$R = \sum_i \left\{ \varepsilon_i - \left(\lambda_\theta \theta_i + \lambda_F F_{di} \right) \right\}^2 \qquad (4)$$

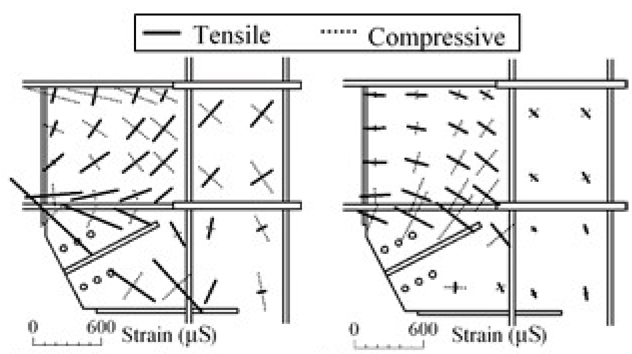

(a) Frame action component at θ=+1/200 (b) Damper action component at F_d =-860kN

Figure 16 Combined test: Decomposition of principal strains recorded at θ=+1/200, F_d=-860kN, and sum of the two components

Equation 4 is applied up to the end of the second cycle of the peak story drift angle $\theta = \pm 1/200$. After obtaining the frame and damper action components, the principal strains and their directions are calculated and plotted. Figure 16 shows such a result at $\theta = +1/200$ rad and $F_d = -860$ kN. These results are analogous to the plots from the separate frame and damper action tests (Figure 14).

Thus, using this method, the contributions of the frame and damper actions can be clarified without conducting separate tests, and the hypothetical case of different balance of the two actions could be modeled. Moreover, using the plots shown in Figure 17, the time history curve of the damper action may be shifted or its shape can be modified to examine the effects on the superimposed responses.

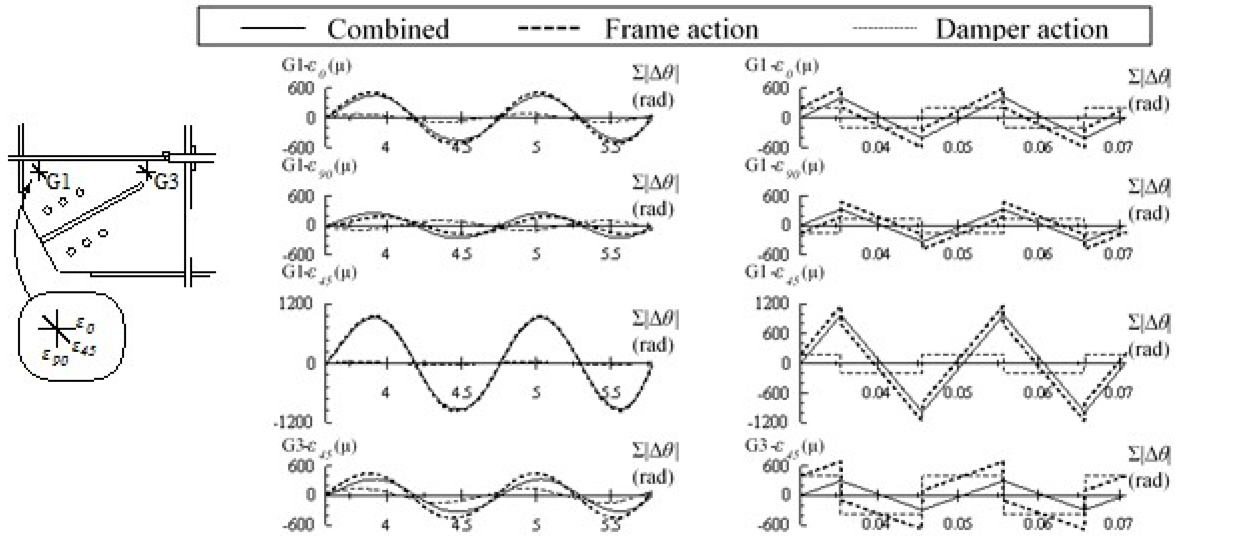

(a) Specimen 2 (VE damper modeled) (b) Specimen 2 (Friction damper modeled)

Figure 17 Composite specimen: Decomposition of strains and their sum

5. CUMULATIVE DAMAGE AND FAILURE MODE

5.1 Cumulative Damage

Figure 18 shows the change in the absolute value of frame shear force Q_f in the positive and negative loading cases. Because Specimen 1 was loaded with multiple cycles of a relatively small story drift angle ($\theta = \pm 1/50$ rad), this specimen underwent a relatively large number of cycles (106 cycles) until failure. In this specimen, local buckling was not remarkable; the frame shear force Q_f in the positive and negative loading cases decreased gradually every cycle, and that in the negative loading case decreased more rapidly. In contrast, Specimen 2, which is a standard specimen like Specimen 1, failed after 47 cycles because it was loaded with multiple cycles of a relatively large story drift angle ($\theta = \pm 1/33$). Specimen 3 is also a standard specimen, but it failed after only 16 cycles. The details of this will be described in Section 5.2.

Specimens 4 and 5 failed after 30 and 17 cycles, respectively, because of their large width-to-thickness ratios. In addition, local buckling occurred early in these specimens, and the decrease in the frame shear force Q_f after every cycle was remarkable. Specimen 6 failed after only 18 cycles because the gusset plate fractured. The details of this failure will be described in Section 5.2.

Specimens 7 and 8 failed after 45 and 43 cycles, respectively, for the same reason as Specimen 2. In addition, the decrease in the frame shear force Q_f after every cycle was not remarkable because of the small beam deformations due to the relatively large connection deformation. In Specimens 9 and 10, local buckling in the beam was not remarkable, and thus Q_f was equal in the positive and negative loading cases.

5.2 Failure mode

Figure 19 shows the failure types. Failure Types A to C include the development of cracks in the bottom flange at the end of the gusset plate and in the weld connecting the bottom flange and the web because of the severe local buckling of both the flange and the web. In these tests, the beam was subjected to axial tension and a positive moment in the positive loading case, and vice versa. Hence, these failure types were the majority.

Specimen 6 showed Failure Type D, in which the tearing of the gusset plate progressed in the horizontal direction from the edge of the vertical side stiffener and gusset plate. Specimen 6, which has a thinner gusset plate, was the only specimen to show Failure Type D.

Specimen 3 showed Failure Type E, which begins with the progression of the delamination of the weld connecting the gusset plate and the vertical side stiffener along the vertical side stiffener, followed by the delamination of the weld connecting the gusset plate and the bottom flange, ultimately resulting in the fracture of the bottom flange. This failure type appears to have been caused by a relatively high shear force Q_f and strain concentration resulting from the tearing of the weld due to the partial penetration of the weld.

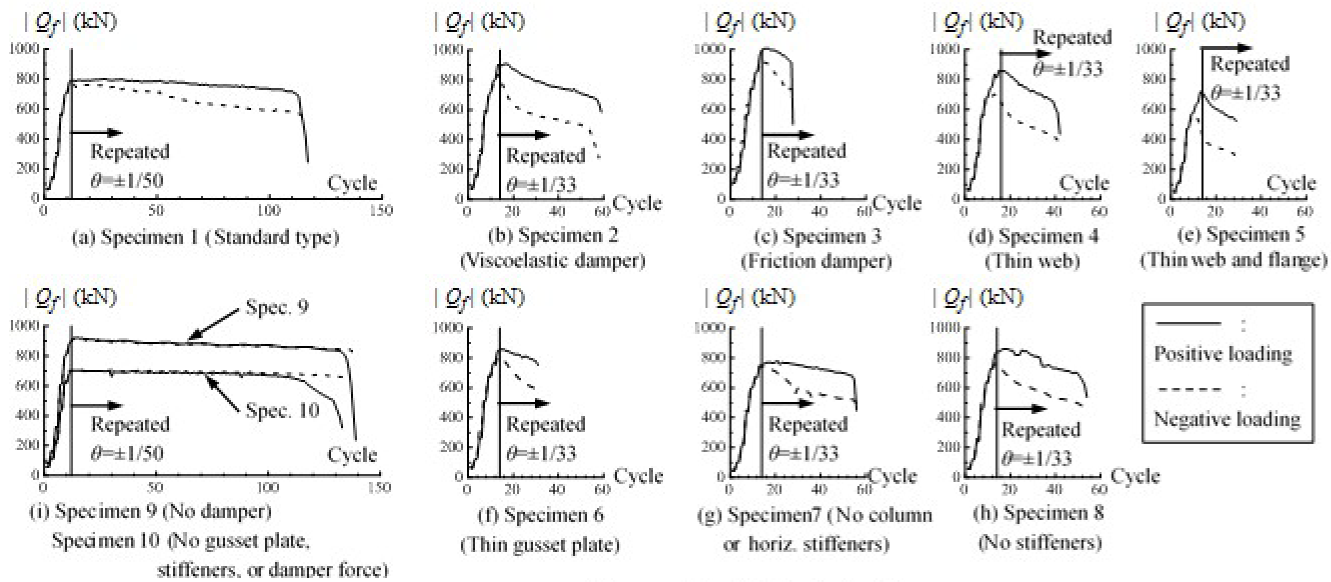

Figure 18 $|Q_f|$ deterioration

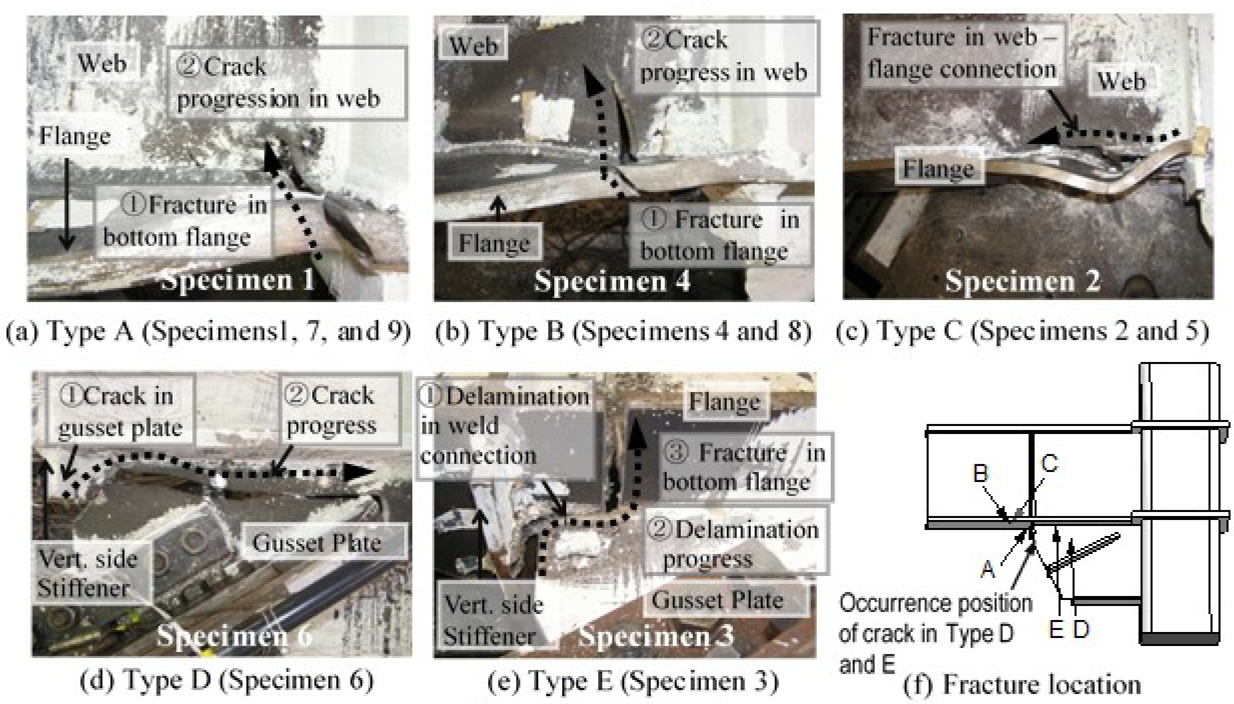

Figure 19 Fracture types

6. CONCLUSION

This paper proposes a full-scale subassembly test simulating the frame and damper actions. To clarify the effects of these actions and different details of the behavior of passively controlled buildings, 10 subassemblies each consisting of a beam, a column, and a gusset plate were tested systematically by varying pertinent parameters. The conclusions are as follows.

1. The proposed test method for the subassembly with simulated frame and damper actions performed well, producing realistic overall hysteresis and local behavior. Simultaneous displacement and force control, connected by the numerical simulation of the damper action, was performed.
2. The horizontal shear forces of the damper, the frame, and the combined system were plotted with respect to story drift angle. Specimens 1, 2, and 3 are standard specimens that experienced simulated steel, viscoelastic, and friction damper forces, respectively. The frame yielded at the beam at a story drift angle cycle of $\theta = \pm 1/100$ rad. The peak force of the specimen with the gusset plate was greater than that of a standard beam–column assembly used for a moment frame because the plastic hinge was shifted to the gusset plate region from the column face.
3. The frame that contained the beam section with the largest width-to-thickness ratios for both the flange and the web exhibited the smallest peak story shear due to local buckling.
4. The specimen with the thinnest gusset plate had a horizontal stiffness similar to that of the standard specimen. However, it suffered from early yielding at a cycle of $\theta = 1/200$ rad, and consequent tearing occurred at the gusset plate in relatively early cycles.
5. In the subassembly without gusset, beam, and column stiffeners, the peak story shear was approximately equal to that of the standard specimen, but the horizontal stiffness was small.
6. Two-dimensional strains at the gusset plate of the subassembly were decomposed, and highly non-uniform strains were clarified by combining the two scaled actions. The contribution of each action was obtained without conducting separate tests, and it was demonstrated that the combined effects can be easily evaluated for the design process.

References

[1] Kasai, K., Hikino, T., Ito, H., Ooki, Y., Kato, F., Baba, Y. (2011). Overall test outline and response of building without dampers, 3D shake table tests on full scale 5-story steel building with dampers Part1. *J. Struct. Constr. Eng.*, No.663, pp.997-1006, Japan.

[2] Kasai, K., Baba, Y., Nishizawa, K., Hikino, T., Ito, H., Ooki, Y., Motoyui, S. (2012). Test results for building with steel dampers, 3D shake table tests on full scale 5-story steel building with dampers Part2. *J. Struct. Constr. Eng.*, No.673, pp. 499-508, Japan.

[3] Kasai, K., Baba, Y., Ito, H., Tokoro, K., Hikino, T., Ooki, Y., Murai, R. (2012). 3-D shake table tests on full scale 5-story steel building with viscoelastic dampers. *J. Struct. Constr. Eng.*, No.676, pp. 985-994, Japan.

[4] Kasai, K., Yamagiwa, H., Baba, Y., Ito, H., Hikino, T., Ooki, Y. (2013). 3-D shake table tests on full scale 5-story steel building with oil dampers. *J. Struct. Constr. Eng.*, No.693, pp. 1999-2008.

[5] Kasai, K. , Yamazaki, H., Kozawa, H., Kaneko, H., Sadasue, K., Ono, Y. (2008). Curved hysteresis model of structural steel under cyclic loading, Part 7 substantially improved analysis model. *Summaries of Technical Papers of Annual Meeting*. Architectural Institute of Japan 2008, C1, pp. 907-908, Japan.

[6] Kasai, K. , Yamazaki, H., Kozawa, H., Kaneko, H., Sadasue, K., Ono, Y. (2008). Curved hysteresis model of structural steel under cyclic loading, Part 7 stress-strain curve of low yield strength steel LY100 considering amplitude and strain velocity dependance. *Summaries of Technical Papers of Annual Meeting*. Architectural Institute of Japan 2008, C1, pp. 909-910, Japan.

[7] Kasai, K., Okuma, K. (2004). Evaluation rule and its accuracy for equivalent period and damping of frequency-dependent passive control systems, Global damping model of one-mass system having elastic frame and either viscoelastic or oil damper. *J. Struct. Constr. Eng.*, No.580, pp.51-59, Japan.

[8] Architecture Institute of Japan (2010). Recommendation for limit state design of steel structure.

[9] Architecture Institute of Japan (2010). Recommendation for design of connection in steel structure.